Please cite this article in press as: Raitano et al., Restoration of Progranulin Expression Rescues Cortical Neuron Generation in an Induced Pluripotent Stem Cell Model of Frontotemporal Dementia, Stem Cell Reports (2015), http://dx.doi.org/10.1016/j.stemcr.2014.12.001

Stem Cell Reports
Report
ISSCR
OPEN ACCESS

Restoration of Progranulin Expression Rescues Cortical Neuron Generation in an Induced Pluripotent Stem Cell Model of Frontotemporal Dementia

Susanna Raitano,[1,2] Laura Ordovàs,[1,2] Louis De Muynck,[3,4,5] Wenting Guo,[3,4,5] Ira Espuny-Camacho,[6,7,8,9] Martine Geraerts,[1,2] Satish Khurana,[1,2] Kim Vanuytsel,[1,2] Balazs I. Tóth,[10] Thomas Voets,[10] Rik Vandenberghe,[3,4,14] Toni Cathomen,[11,12] Ludo Van Den Bosch,[3,4,5] Pierre Vanderhaeghen,[6,7,8,9,13] Philip Van Damme,[3,4,5,14,15] and Catherine M. Verfaillie[1,2,15,*]

[1]Stem Cell Institute, KU Leuven, 3000 Leuven, Belgium
[2]Stem Cell Biology and Embryology Unit, Department of Development and Regeneration, KU Leuven, 3000 Leuven, Belgium
[3]Leuven Research Institute for Neuroscience and Disease (LIND), KU Leuven, 3000 Leuven, Belgium
[4]Research Group Experimental Neurology, Department of Neurosciences, KU Leuven, 3000 Leuven, Belgium
[5]Laboratory of Neurobiology, VIB Vesalius Research Center, 3000 Leuven, Belgium
[6]Institute for Interdisciplinary Research (IRIBHM), Université Libre de Bruxelles (ULB), 1070 Brussels, Belgium
[7]Institute of Neuroscience (UNI), ULB, 1070 Brussels, Belgium
[8]VIB Center for the Biology of Disease, 3000 Leuven, Belgium
[9]Center of Human Genetics, KU Leuven, 3000 Leuven, Belgium
[10]Laboratory of Ion Channel Research, KU Leuven, 3000 Leuven, Belgium
[11]Institute for Cell and Gene Therapy, University Medical Center, 79108 Freiburg, Germany
[12]Center for Chronic Immunodeficiency, University Medical Center, 79108 Freiburg, Germany
[13]Walloon Excellence in Life Sciences and Biotechnology (WELBIO), 1070 Brussels, Belgium
[14]Department of Neurology, University Hospitals Leuven, 3000 Leuven, Belgium
[15]Co-senior author
*Correspondence: catherine.verfaillie@med.kuleuven.be
http://dx.doi.org/10.1016/j.stemcr.2014.12.001

SUMMARY

To understand how haploinsufficiency of progranulin (PGRN) causes frontotemporal dementia (FTD), we created induced pluripotent stem cells (iPSCs) from patients carrying the *GRN*$^{IVS1+5G > C}$ mutation (FTD-iPSCs). FTD-iPSCs were fated to cortical neurons, the cells most affected in FTD. Although generation of neuroprogenitors was unaffected, their further differentiation into CTIP2-, FOXP2-, or TBR1-TUJ1 double-positive cortical neurons, but not motorneurons, was significantly decreased in FTD-neural progeny. Zinc finger nuclease-mediated introduction of *GRN* cDNA into the *AAVS1* locus corrected defects in cortical neurogenesis, demonstrating that PGRN haploinsufficiency causes inefficient cortical neuron generation. RNA sequencing analysis confirmed reversal of the altered gene expression profile following genetic correction. We identified the Wnt signaling pathway as one of the top defective pathways in FTD-iPSC-derived neurons, which was reversed following genetic correction. Differentiation of FTD-iPSCs in the presence of a WNT inhibitor mitigated defective corticogenesis. Therefore, we demonstrate that PGRN haploinsufficiency hampers corticogenesis in vitro.

INTRODUCTION

Frontotemporal dementia (FTD) accounts for ~50% of dementia cases before the age of 60. Up to 40% of FTD patients have a familial history (Goldman et al., 2005; van Swieten and Heutink, 2008) due to mutations in the microtubule-associated protein tau gene (*MAPT*), progranulin gene (*GRN*), or *C9orf72* gene (Baker et al., 2006; Cruts et al., 2006; DeJesus-Hernandez et al., 2011; Hutton et al., 1998; Renton et al., 2011). The majority of FTD-causing mutations in *GRN* are predicted to result in functional null alleles, causing haploinsufficiency. Progranulin (PGRN) has neurotrophic function in vitro and in vivo. Although PGRN$^{-/-}$ mice are viable, they do not recapitulate all the features of FTD (Kayasuga et al., 2007).

Human somatic cell reprogramming to a pluripotent state (induced pluripotent stem cells; iPSCs)(Takahashi et al., 2007a) can create human disease models in vitro using patient-derived iPSCs (Kim, 2014), including neurodegenerative diseases (Qiang et al., 2013) and, specifically, FTD (Almeida et al., 2012). Unlike in the published FTD-iPSC model that differentiated iPSCs to a mixture of neuronal cells, we evaluated cortical neuron development from FTD-patient-derived iPSCs, as FTD is characterized by selective neurodegeneration of the frontal and/or temporal cortex (Neary et al., 2005). We demonstrate that FTD-iPSCs carrying a *GRN*$^{IVS1+5G > C}$ mutation differ in their ability to generate cortical neurons from control lines (iPSCs and human embryonic stem cells; hESCs) and that genetic correction restores this differentiation defect.

RESULTS

FTD-iPSCs Differentiation into Neuroprogenitors Is Normal

To study the effect of PGRN haploinsufficiency in human neurogenesis, iPSC lines were generated from three

different patients carrying the *GRN*$^{IVS1+5G > C}$ mutation (Figure S1A available online) as previously described (Takahashi et al., 2007b). The human embryonic stem cell line, H9 (H9-ESC), and iPSCs from normal donor fibroblasts (CTRL-iPSCs) were used as control lines (Figures S1B–S1E). Transcript and protein levels of PGRN in FTD-iPSC lines were reduced, approximately 30% and 50%, respectively, compared to H9-hESCs and CTRL-iPSCs (Figures S1F and S1G). We next induced cortical differentiation (Espuny-Camacho et al., 2013), which induced an increase in transcripts for the neuroprogenitor genes *SOX1*, *PAX6*, and *FABP7* (*BLBP*), with concomitant decrease in *OCT4* expression in day (d)24 FTD-iPSCs as well as CTRL-iPSC and H9-hESC progeny (Figure S2A). Immunostaining confirmed that d24 neuroprogenitors did not express OCT4. Nearly 100% of the progeny of all lines were positive for the neuroectoderm-specific NESTIN marker, with a PAX6-positive dorsal fate, and stained positive for BLBP and OTX1-2 (Figure S2B). Thus, neuroprogenitor formation from FTD-iPSCs appeared normal.

Inefficient Cortical Neuron Formation from FTD-iPSCs

We next allowed the neuroprogenitors to mature into cortical neurons. *GRN* mRNA levels in FTD cells during differentiation were approximately 50% compared to control lines (Figure 1A). D40 progeny from CTRL- and FTD-iPSCs contained functional neurons based on whole-cell current-clamp analysis. FTD-iPSC neurons consistently fired action potentials in response to depolarizing current injections, similar to neurons from control cell lines (Figures S2CI–S2CII). Whole-cell voltage-clamp recordings revealed time- and voltage-dependent currents during depolarizing voltage steps, consistent with functional voltage-gated Na^+ and K^+ channels (Figure S2CIII). The cortical neurotransmitter GABA induced transmembrane currents in FTD-iPSC-derived neurons, exhibiting the typical features of ionotropic $GABA_A$ receptors (Figure S2CIV). We also observed spontaneous action potential firing in FTD-iPSC neurons (Figure S2CV). Thus, FTD-iPSC neuroprogenitors were able to differentiate into functional, excitable neurons.

Between d24 and d40 of differentiation, transcript levels of *REELIN*, *CTIP2*, *FOXG1*, *FOXP2*, and *TBR1* progressively increased in neural progeny from FTD- and CTRL-iPSC lines. However, on d40, *CTIP2* and *FOXG1* mRNA levels were significantly lower in FTD-iPSC than in CTRL-iPSC progeny (Figures 1B and S2D). Also, mature TUJ1-positive neurons coexpressed the cortical markers TBR1, FOXP2, and CTIP2. However, compared to CTRL-iPSC and H9-hESC progeny, only a small fraction of FTD-iPSC progeny was positive for TUJ1 (CTRL-iPSCs, 20.7% ± 3.1%; FTD-iPSCs, 4.0% ± 0.69%) (Figures 1C and 1D). In both CTRL-iPSC and FTD-iPSC progeny, a proportion of undifferentiated NESTIN-positive neuroprogenitors persisted till d40 (Figure 1E). Thus, using a cortical neuron differentiation protocol, we demonstrate significantly decreased corticogenesis from FTD-iPSCs.

To test if the neurogenesis defect was specific for cortical neuron generation, FTD-iPSCs and hESCs were differentiated to motor neurons (Hu and Zhang, 2009). Immunostaining for the mature motor neuron markers *HB9* and *ISLET1* (Figure 1F) demonstrated that FTD3-iPSCs generated motor neurons in vitro. Thus, in contrast to what we observed during cortical neuron differentiation, motor neuron generation from FTD-iPSCs was not affected.

We stained cortical neuron progeny for activated caspase-3 but found no significant differences in the number of apoptotic cells between FTD and CTRL lines (Figure S2E). As *GRN* mutations in humans lead to accumulation of TDP-43-positive inclusions, we performed TDP-43 staining, which did not identify TDP-43 aggregates, and TDP-43 displayed a nuclear staining in all cells (Figure S2F).

Genetic Correction of FTD-iPSCs Restores PGRN Levels

To study the relationship between PGRN haploinsufficiency and the phenotype observed, we introduced *GRN* cDNA by homologous recombination with zinc finger nucleases (ZFNs) in the *AAVS1* locus of FTD3#6-iPSCs (Figure 2A). To identify correct targeting and absence of random integrations, we performed genotyping based on PCR and Southern blot analysis (Figures 2B and 2C). One correctly homozygously targeted clone (#9) derived from the FTD3#6 line (hereinafter referred to as FTD3#6-PGRN) was chosen for complete characterization. As an additional control, we recombined the *GRN* cDNA into the *AAVS1* locus of H9-hESCs (H9-hESC-PGRN) (Figure S3A).

GRN transcript levels in FTD3#6-PGRN and H9-hESC-PGRN cells were not significantly different from that in H9-hESCs (Figure 2D). FTD3#6-PGRN cells expressed the pluripotency markers at levels comparable to that of H9-hESCs (Figures 2E and 2F) and formed teratomas (Figure 2G). Genome integrity of FTD3#6-PGRN, assessed by array comparative genomic hybridization, revealed no significant acquired genetic abnormalities after gene editing, compared to the original line.

Genetic Correction of FTD-iPSCs Restores Cortical Neuron Formation

We differentiated FTD3#6-iPSC, FTD3#6-PGRN, H9-hESC, and H9-hESC-PGRN lines to cortical neurons. Patch clamp recording confirmed the functional maturity of FTD3#6-PGRN and H9-hESC-PGRN neurons (data not shown). Differentiation toward neuroprogenitors until d24 was similar for the FTD3#6, FTD3#6-PGRN, H9-ESC, and H9-PGRN lines, as shown by immunostaining for neuroprogenitor markers (Figure S3B) and quantitative RT-PCR (Figure S3C).

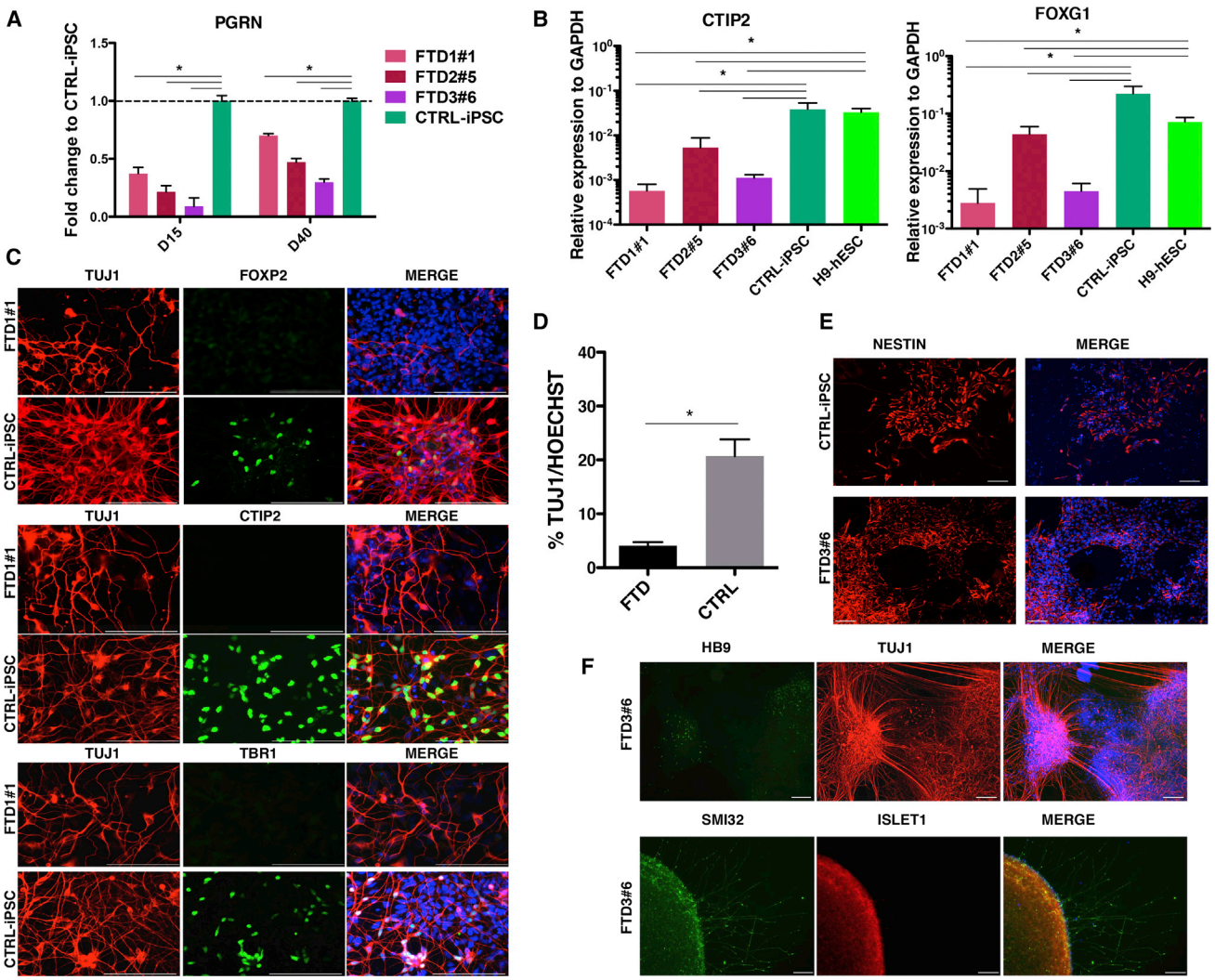

Figure 1. Generation of Cortical Neurons from FTD-iPSCs and CTRL Lines

(A) *GRN* levels in FTD-iPSC lines compared to those in control CTRL-iPSC lines (n = 3 independent experiments). Error bars indicate mean ± SEM. *p < 0.05, t test.

(B) *CTIP* and *FOXG1* expression in d40 progeny of FTD-iPSC and CTRL lines (n = 3 independent experiments). Error bars indicate mean ± SEM. *p < 0.05, t test.

(C) Immunostaining for TUJ1 and the cortical markers TBR1, CTIP2, and FOXP2. FTD1#1-iPSC and CTRL-iPSC progeny at d40 are shown. Scale bar, 100 μm.

(D) Enumeration of TUJ1-positive cells in FTD-iPSC and CTRL-iPSC d40 progeny. FTD1#1 and FTD3#6 (FTD) lines and CTRL-iPSC and H9-hESC (CTRL) lines are shown (n = 3 independent experiments per line. Error bars indicate mean ± SEM. *p < 0.05, t test.

(E) Immunostaining on d40 progeny for Nestin (n = 3). Scale bar, 100 μm.

(F) Immunostaining of FTD3#6 on d40 of differentiation to motorneurons for TUJ1, SMI32, HB9, and ISLET1 (n = 2). Scale bar, 100 μm. See also Figures S1 and S2.

However, compared with FTD3#6, d40 FTD3#6-PGRN progeny expressed significantly higher *BLBP*, *FOXG1*, and *CTIP2* transcript levels, which were similar to those in H9-hESC and H9-hESC-PGRN progeny (Figure 3A; Figure S3C). Immunostaining for TUJ1 and the cortical neuron markers CTIP2, FOXP2, and TBR1 demonstrated that more double-positive cells were present in progeny from the FTD3#6-PGRN line compared to the original isogenic line FTD3#6 (Figure 3B). Quantification of the number of $TUJ1^+$ and $CTIP2^+$ neurons demonstrated that FTD3#6-PGRN iPSC progeny contained significantly more $TUJ1^+$ and $CTIP2^+$ neurons compared with FTD3#6 and that genetic correction partially rescued the frequency of neurons generated compared to CTRL-iPSCs

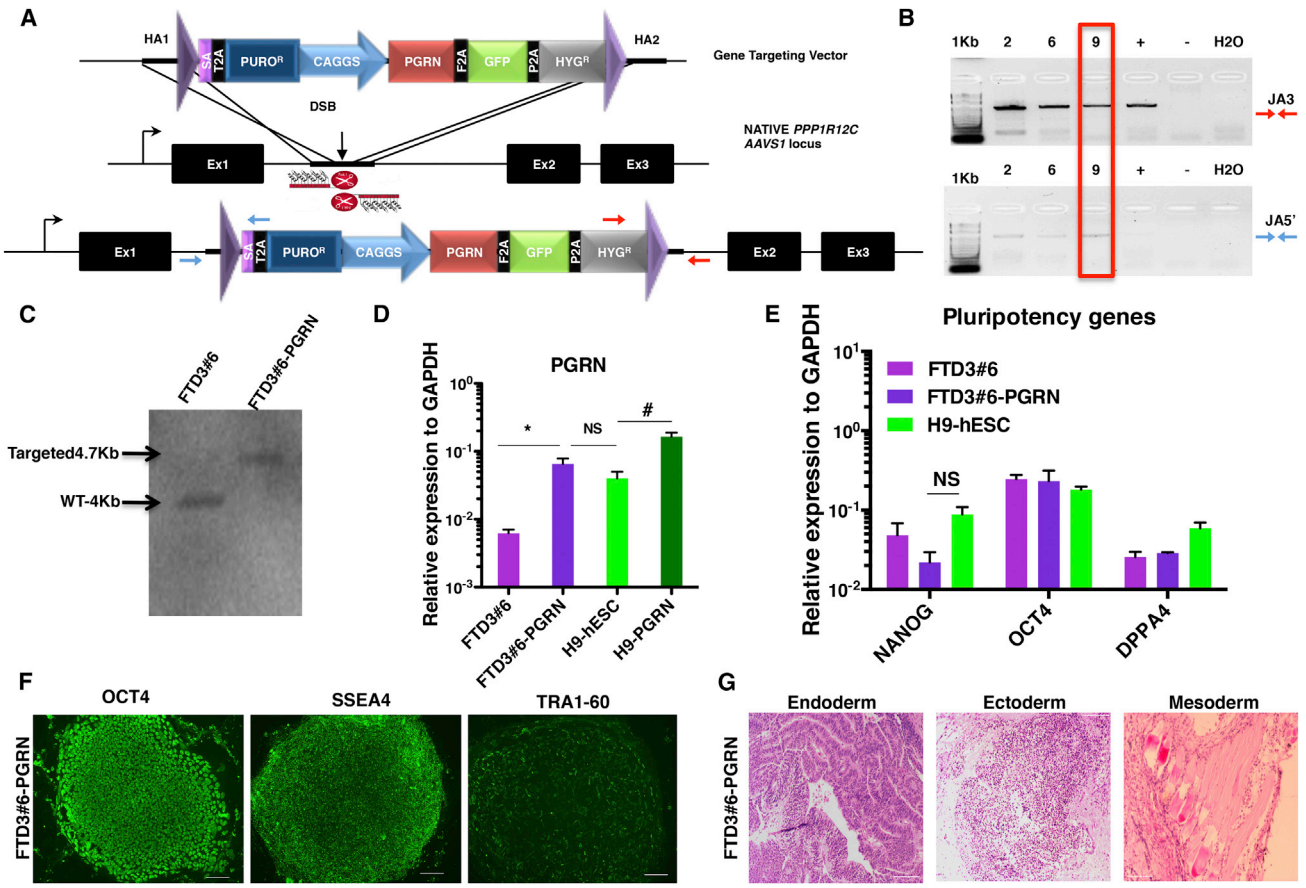

Figure 2. Gene Targeting Using ZFNs

(A) Schematic representation of *GRN* gene targeting in the *AAVS1* locus. HA, homology arm; CAGGS, chicken β-actin promoter; HYG^R, hygromycin resistance-thymidine kinase fusion gene. Blue arrows, primers designed for junction assay (JA) PCR at the 5′ of the construct; red arrows, PCR for JA at the 3′. $PURO^R$, puromycin resistance.

(B) JA-PCR for several clones; the clone number 9 was selected. +, positive control for 3′ JA (engineered H9-hESC line created by L.O. [unpublished data]); −, negative control (FTD-iPSC not targeted).

(C) Southern blot of FTD3#6 and FTD3#6-PGRN lines.

(D) *GRN* expression in FTD3#6, H9-hESC, FTD3#6-PGRN, and H9-PGRN lines (NS, not significant, p = 1.6, t test; n = 3 different passages). Error bars indicate mean ± SEM. $^{\#}p = 0.07$; $^{*}p < 0.05$, t test.

(E) *NANOG*, *OCT4*, and *DPPA4* expression in FTD3#6, FTD3#6-PGRN, and H9-hESC lines (NS, not significant, p = 0.26, t test; n = 3 different passages). Error bars indicate mean ± SEM.

(F) Immunostaining of FTD3#6-PGRN for OCT4, SSEA4, and TRA1-60 (n = 3). Scale bar, 100 μm.

(G) FTD3#6-PGRN-derived teratoma with presence of derivatives of all three germ layers. Scale bar, 500 μm.

See also Figure S3.

(TUJ1: CTRL-iPSC, 23.7% ± 3.8%, FTD3#6-PGRN, 9.4% ± 1.4%, and FTD3#6, 3.2 %± 0.3%; CTIP2: CTRL-iPSC, 14.2% ± 2.2%, FTD3#6-PGRN 6.2, ± 1.9%, and FTD3#6, 1.6% ± 0.5%) (Figure 3C). Hence, incorporation of *GRN* cDNA in the *AAVS1* locus restored the ability of FTD-iPSCs to differentiate to functional neurons with a cortical fate. As the presence of an extra copy of *GRN* in H9-hESCs did not affect the differentiation potential of H9-hESCs, our studies indicate that deficiency of PGRN is the cause of the in vitro impaired cortical neuron generation from FTD-iPSCs. Incorporation of *GRN* cDNA in the *AAVS1* locus of FTD3#6 iPSCs did not affect motor neuron differentiation (Figures 3D and 3E).

Genome-wide Transcriptome Analysis of d40 Neuronal Progeny Identifies Increased Wnt Signaling

To gain insights in possible mechanisms underlying the inefficient cortical neuron generation from FTD-iPSCs, we performed RNA sequencing (RNA-seq) of d40 progeny from FTD3#6, FTD3#6-PGRN, and H9-hESC lines. We

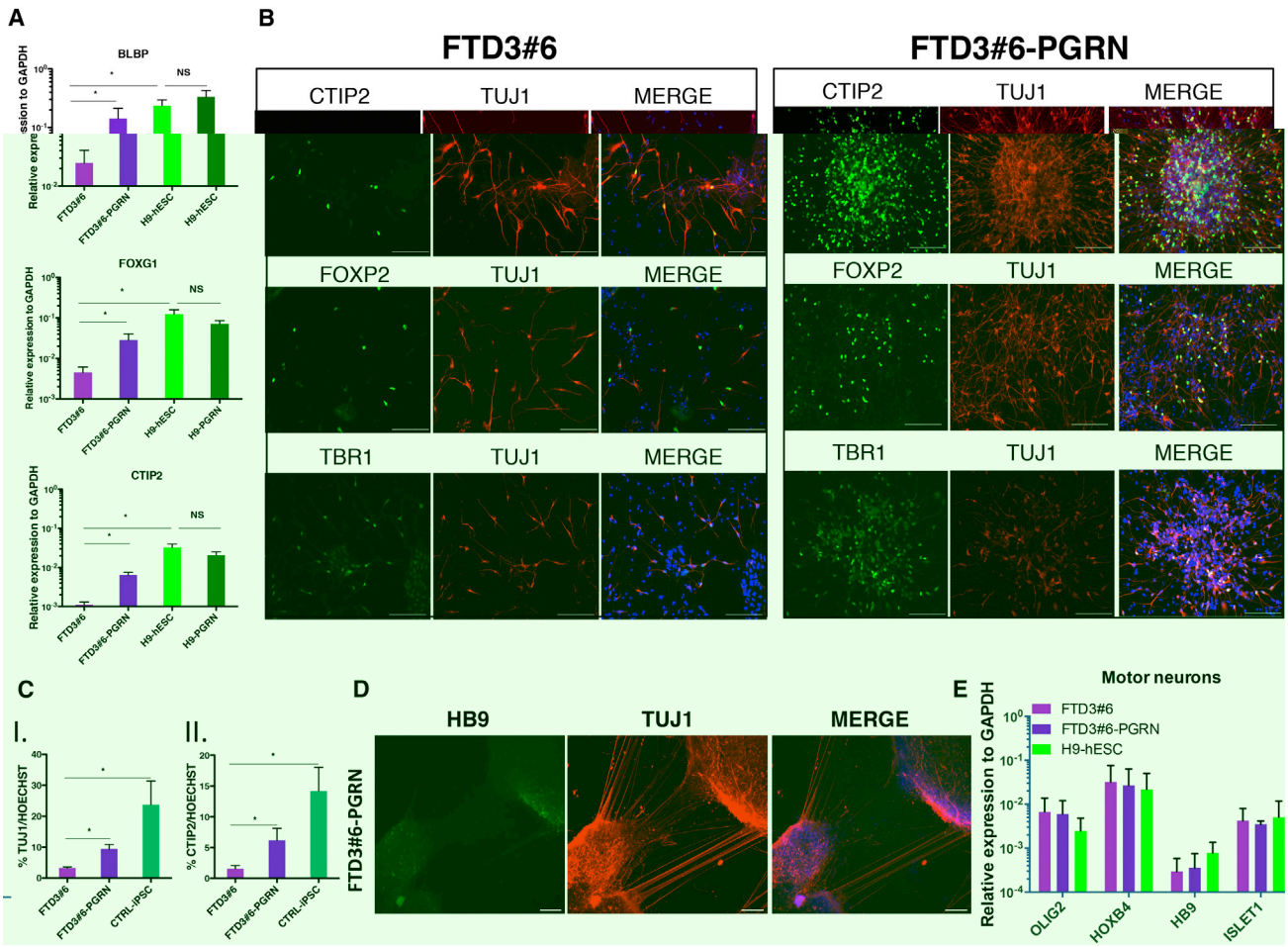

Figure 3. Rescue of Corticogenesis in FTD3#6-PGRN Cells

(A) *BLBP*, *FOXG1*, and *CTIP2* expression in FTD3#6-PGRN, FTD3#6-iPSC, H9-hESC, and H9-PGRN lines (n = 3 independent experiments). NS, not significant; p = 0.28, p = 0.23, p = 0.2 for top, middle, and bottom panels, respectively, t test. Error bars indicate mean ± SEM. *p < 0.05, t test.

(B) Immunostaining of FTD3#6 and FTD3#6-PGRN for TUJ1 and CTIP2, FOXP2, and TBR1 (n = 3). Scale bars, 100 μm.

(C) Enumeration of TUJ1-positive (I) and CTIP2-positive cells (II) in d40 progeny from FTD3#6-PGRN iPSCs compared to FTD3#6 and CTRL-iPSC lines (n = 3 independent experiments per line). Error bars indicate mean ± SEM. *p < 0.05, t test.

(D) Immunostaining of FTD3#6-PGRN for TUJ1 and HB9 (n = 2). Scale bar, 100 μm.

(E) Transcript levels of motorneuron precursor and mature markers (n = 2 independent experiments). Error bars indicate mean ± SEM. See also Figure S3.

identified 2,295 genes differentially expressed between d40 progeny of FTD3#6 and H9-hESCs, whereas only 122 genes were differentially expressed between the FTD3#6-PGRN and the H9-hESC progeny (Figure 4A).

RNA-seq data corroborated our observation that cortical neuronal differentiation from FTD-iPSCs is inefficient, as here too, *TUBB3*, *CTIP2*, *FOXG1*, *BLBP*, and *MAP2* were significantly downregulated in FTD3#6, compared to H9-hESC progeny, and restored in FTD3#6-PGRN progeny (Figure 4B). Although we did not see an increase in apoptotic cells, the RNA-seq data demonstrated that, in line with the findings in the Almeida et al. (2012) paper, some components of the MAPK pathway were differentially expressed in the d40 progeny of FTD3#6 cells compared with FTD3#6-PGRN and H9-hESC progeny (Figure S4A).

Gene ontology analysis using DAVID demonstrated that "neurogenesis," "generation of neurons," "neuron development," "neuron projection development," and "synaptic transmission" were within the top "Biological Processes" categories significantly enriched in FTD3#6 versus H9-hESC progeny and in FTD3#6-PGRN versus FTD3#6 progeny. Ingenuity pathway analysis identified Wnt/β-catenin signaling as one of the top altered pathways. Among other genes, *WNT2*, *WNT3a*, *WNT5a*,

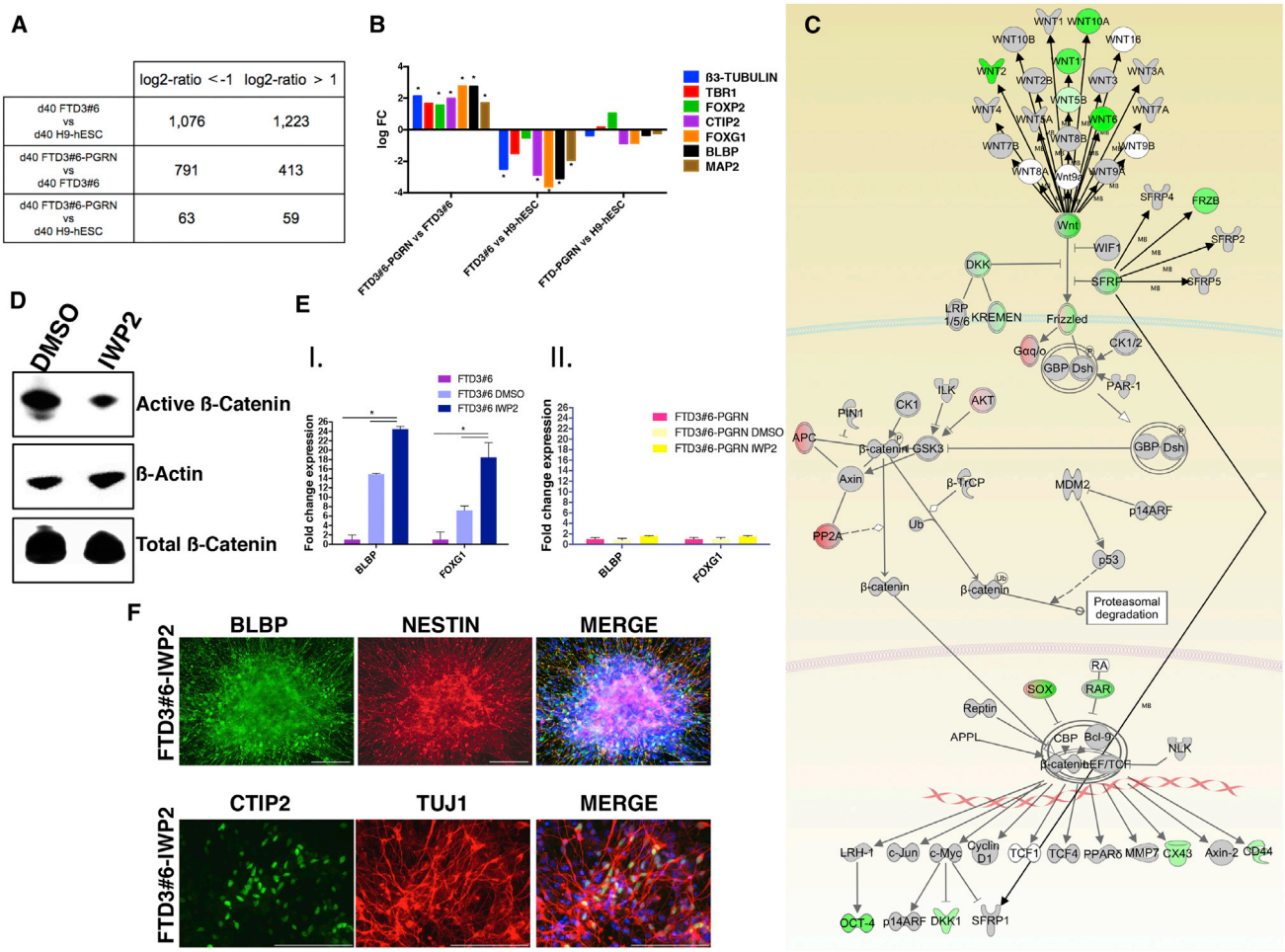

Figure 4. Genome-wide Transcriptome Analysis of d40 Neuronal Progeny

(A) Table with the significantly differentially expressed genes (using Benjamini-Hochberg-corrected p values).

(B) Represents the log fold change of gene transcripts of *TUBB3*, *TBR1*, *FOXP2*, *CTIP2*, *FOXG1*, *BLBP*, and *MAP2* in d40 neural progeny of the FTD3#6, H9-hESC, and FTD3#6-PGRN lines from RNA-seq studies.

(C) Wnt signaling pathway, overlaid with the differentially expressed genes (log_2 ratio >1 or <−1) of FTD3#6 versus H9-hESC line comparison. Upregulated genes are in green, and downregulated genes are in red.

(D) Western blot for active and total β-catenin on H9-hESCs at d24 treated with DMSO or DMSO-IWP2 (IWP2). β-actin, internal control.

(E) Panel I: Relative expression of *BLBP* and *FOXG1* transcripts in FTD3#6 treated with or without DMSO and IWP2 (n = 3 independent experiments). Error bars indicate mean ± SEM; *p < 0.05, t test. Panel II: *BLBP* and *FOXG1* transcripts in FTD3#6-iPSC treated with DMSO or DMSO-IWP2 (IWP2). n = 3 independent experiments. Error bars indicate mean ± SEM. *p < 0.05, t test.

(F) Immunostaining on FTD3#6 d40 progeny treated with DMSO-IWP2 (IWP2) for NESTIN and BLBP or TUJ1 and CTIP2 (n = 3). Scale bars, 100 μm.

See also Figure S4.

WNT6, and *WNT10a; CTNNB1; LEF/TCF* were more highly expressed in FTD3#6 compared to FTD3#6-PGRN and H9-hESC progeny, while *GSK3β*, *APC*, and *PP2A* were expressed significantly less in FTD3#6-iPSC progeny. However, expression of genes from the WNT signaling pathway was similar in FTD3#6-PGRN compared with H9-hESC neural progeny (Figures 4C and S4B).

To address whether aberrantly activated WNT signaling was, at least in part, responsible for the defective corticogenesis, we induced cortical neuron differentiation of FTD3#6, FTD3#6-PGRN, and H9-ESC lines in the presence or absence of the WNT inhibitor, IWP2. Western blot analysis demonstrated that IWP2 inhibited active β-catenin levels (Figure 4D). On d40 of differentiation, transcript levels for *BLBP* and *FOXG1* were significantly higher in FTD3#6 progeny treated with IWP2, dissolved in DMSO, compared to FTD3#6 treated with DMSO and untreated cells (Figures 4E–4I). Of note, addition of DMSO alone

also enhanced expression of *BLBP* and *FOXG1* in FTD3#6 progeny, while IWP2 induced a further significant increase in these transcripts. The increased frequency of neurons in DMSO-treated FTD-iPSC progeny is possibly an indirect effect of DMSO-induced PGRN upregulation, as previously reported (Ong et al., 2006). Consistent with this notion, addition of DMSO (and IWP2) to differentiation of FTD3#6-PGRN (Figure 4EII) or H9-hESC (data not shown) lines did not affect expression of cortical neuron markers. Immunostaining demonstrated that more BLBP- and CTIP2-positive cells were generated when IWP2 was added during the cortical neuron differentiation of FTD3#6 cells (Figure 4F). Again, this improvement was also visible in the DMSO-treated cells (data not shown).

DISCUSSION

We demonstrate that iPSCs generated from FTD patients carrying a *GRN IVS1+5G > C* null mutation poorly differentiate to cortical neurons, while differentiation to motor neurons appears normal. Introduction of the *GRN* cDNA in the *AAVS1* locus of FTD-iPSCs using ZFN-mediated homologous recombination corrected the inefficient cortical neuron generation. Loss of PGRN caused aberrant activation of the WNT signaling pathway during neuronal differentiation, and inhibition of WNT signaling partially rescued the FTD-iPSC corticogenesis defect, further substantiating the notion that the WNT signaling pathway might be a therapeutic target for FTD (Korade and Mirnics, 2011).

Almeida et al. (2012) previously demonstrated that GRN^{S116X}-iPSCs could be differentiated toward neurons with a similar efficiency as that of control iPSCs but that GRN^{S116X}-iPSCs were more sensitive to stress. We chose to differentiate neuronal progenitors from iPSC lines specifically toward the cortical lineage, as we hypothesized that evaluation of the influence of PGRN haploinsufficiency on cortical neurons, the most affected cell type in FTD, would likely yield the most important insights into the disease. We induced cortical neuron differentiation and demonstrated that generation of TUJ1-positive cells coexpressing cortical markers such as CTIP2, FOXP2, and TBR1 was significantly decreased in FTD-iPSCs. By contrast, Almeida et al., who differentiated iPSCs sequentially as embryoid bodies and neurospheres with additional growth factors to generate a mixture of glutamatergic, GABAergic, and dopaminergic neurons, did not observe decreased cell differentiation. We hypothesize that the differences in the efficiency of neural progeny generation between the two studies might be caused by the specific subtype of neuronal cells we generated. In fact, generation of HB9/TUJ1- and ISLET-1/SMI32-positive motor neurons appeared similar when FTD-iPSC or H9-hESC lines were differentiated to motor neurons.

The role of PGRN in cortical neurons is currently not well understood. PGRN exerts neurotrophic properties through a yet-unidentified receptor (De Muynck et al., 2013; Gass et al., 2012; Van Damme et al., 2008). However, a strong link between PGRN and the WNT signaling pathway in neuronal physiology has been established. Rosen et al. (2011), demonstrated that *GRN* knockdown in primary human neurons activated the canonical and noncanonical WNT signaling pathway. They also found similar WNT signaling activation in transcriptome studies of human *GRN* mutant brain. Furthermore, knockdown of *GRN* in a neural progenitor cell line was shown to inhibit the level of phosphorylated GSK3β, resulting in canonical WNT signaling activation and hampered retinoic-acid-mediated neural differentiation in human cells (Gao et al., 2010).

WNT signaling is also important for pre- and postnatal neuronal development. WNT signaling inhibits neuroectoderm and forebrain specification (Ming and Song, 2011). Postnatally, WNT regulates proliferation and maturation of neural progenitors in the hippocampus and dentate gyrus (Miranda et al., 2012; Wexler et al., 2009). These studies identify a very important role of WNT signaling during brain development, as well as neurogenesis and neural maturation postnatally.

Transcriptome studies on cortical neuron progeny from FTD-iPSCs and isogenic genetically corrected FTD-iPSC and CTRL lines revealed that WNT signaling was among the top canonical signaling pathways deregulated by *GRN* haploinsufficiency. This may explain the decrease in mature cortical neurons generated, as WNT signaling was shown to affect proliferation and maturation of cortical neuronal progenitors (Wexler et al., 2009). However, we could not identify aberrant activation of the WNT signaling pathway in the Almeida et al. (2012) transcriptome studies (Figure S4C), which may, again, be due to differences in neurons generated.

We also demonstrated that aberrant WNT signaling is, at least partly, responsible for the defective in vitro corticogenesis, based on differentiations wherein we added the WNT inhibitor IWP2, which inhibits WNT processing and secretion. WNT signaling abnormalities, observed in our study, are also seen in brains of 6-week-old $Grn^{-/-}$ mice (Rosen et al., 2011) before the occurrence of neuroinflammation or neuronal apoptosis, suggesting that aberrant WNT signaling may be an early event in FTD development. Future studies to assess whether spontaneous apoptosis occurs in FTD-iPSC neurons maintained for longer periods of time, and whether this can be linked to aberrant WNT signaling, will be of interest.

We found that in vitro corticogenesis is decreased in $GRN^{IVS1+5G > C}$-iPSCs; however, brain development in

Grn$^{+/-}$ and *Grn*$^{-/-}$ mice and in PGRN haploinsufficient patients appears normal. The reason for the discrepancies in vitro and in vivo might be that excess of WNT signaling during early steps of development can be compensated by other morphogens or cellular interactions, not present in the culture system. However, it is interesting that in patients with FTD, evidence of presymptomatic changes exists (Li et al., 2007).

Neurodegenerative diseases were thought to not be readily recreated in vitro, as they are late-onset diseases. However, several papers have shown that disease phenotypes recapitulated to some extent, using iPSCs (Qiang et al., 2013). This suggests that cellular and molecular causes of these diseases of aging may often already be present earlier during life and that additional events ultimately lead to the full manifestation of the symptoms of the disease. In addition, published studies, as well as the study presented here, suggest that signaling events required for neurodevelopment may also play major roles in neurodegeneration and that targeting such pathways—as for instance, the WNT pathway presented in this study—may result in the creation of novel therapeutic approaches for FTD.

EXPERIMENTAL PROCEDURES

Primary human fibroblast cultures were obtained from skin biopsies of FTD patients after informed consent; control iPSCs were generated from BJ fibroblasts. Human iPSC lines were generated and characterized as previously described (Takahashi et al., 2007b). hESC and iPSC lines were differentiated toward cortical or motor neuron progeny as previously described (Espuny-Camacho et al., 2013; Hu and Zhang, 2009). Gene targeting was performed by use of ZFN technology in the *AAVS1* locus of iPSCs.

For further information, see the Supplemental Experimental Procedures.

SUPPLEMENTAL INFORMATION

Supplemental Information includes Supplemental Experimental Procedures and four figures and can be found with this article online at http://dx.doi.org/10.1016/j.stemcr.2014.12.001.

AUTHOR CONTRIBUTIONS

C.M.V. and P.V.D. planned the project. S.R., L.O., C.M.V., P.V.D., M.G., and L.D.M. participated in the study design, planning, and interpretation of the experiments. L.D.M. performed the ELISA experiments and sequencing of GRN gene in iPSCs and analyzed RNA-seq data. K.V. generated and characterized the CTRL-iPSC line. W.G. performed the motor neuron differentiations, and L.V.D.B. helped in the interpretation of these results. T.C. provided the *AAVS1* ZFN. S.K. and L.D.M. provided scientific discussions and helped with data interpretation. P.V. and I.E-C. provided a training course for cortical neuron generation and helped with the interpretation of data. B.I.T. and T.V. performed patch-clamp analysis and contributed in writing the manuscript. R.V. provided patient samples. S.R. and C.M.V. wrote the manuscript.

ACKNOWLEDGMENTS

We thank the families of the patients who participated in this study. We also thank Mr. Javed Manesia and Dr. Maria Elena Pistoni for their critical help in the review of the data, Prof. Tanya Roskams for the analysis of the teratomas, and Dr. Anja Hasche for her expertise in WNT signaling. T.C. is a consultant for CRISPR Therapeutics. The work was supported by FWO grants G.0832 (to C.M.V. and P.V.) and G.0667.07 (to C.M.V.), by grants from KU Leuven (EIW-B4855-EF/05/11, ETH-C1900-PF, and EME-C2161-GOA/11/012 to C.M.V.) and by a BELSPO-IUAP-DEVREPAIR grant to C.M.V.

Received: July 4, 2014
Revised: November 28, 2014
Accepted: December 1, 2014
Published: December 31, 2014

REFERENCES

Almeida, S., Zhang, Z., Coppola, G., Mao, W., Futai, K., Karydas, A., Geschwind, M.D., Tartaglia, M.C., Gao, F., Gianni, D., et al. (2012). Induced pluripotent stem cell models of progranulin-deficient frontotemporal dementia uncover specific reversible neuronal defects. Cell Reports *2*, 789–798.

Baker, M., Mackenzie, I.R., Pickering-Brown, S.M., Gass, J., Rademakers, R., Lindholm, C., Snowden, J., Adamson, J., Sadovnick, A.D., Rollinson, S., et al. (2006). Mutations in progranulin cause tau-negative frontotemporal dementia linked to chromosome 17. Nature *442*, 916–919.

Cruts, M., Gijselinck, I., van der Zee, J., Engelborghs, S., Wils, H., Pirici, D., Rademakers, R., Vandenberghe, R., Dermaut, B., Martin, J.J., et al. (2006). Null mutations in progranulin cause ubiquitin-positive frontotemporal dementia linked to chromosome 17q21. Nature *442*, 920–924.

De Muynck, L., Herdewyn, S., Beel, S., Scheveneels, W., Van Den Bosch, L., Robberecht, W., and Van Damme, P. (2013). The neurotrophic properties of progranulin depend on the granulin E domain but do not require sortilin binding. Neurobiol. Aging *34*, 2541–2547.

DeJesus-Hernandez, M., Mackenzie, I.R., Boeve, B.F., Boxer, A.L., Baker, M., Rutherford, N.J., Nicholson, A.M., Finch, N.A., Flynn, H., Adamson, J., et al. (2011). Expanded GGGGCC hexanucleotide repeat in noncoding region of C9ORF72 causes chromosome 9p-linked FTD and ALS. Neuron *72*, 245–256.

Espuny-Camacho, I., Michelsen, K.A., Gall, D., Linaro, D., Hasche, A., Bonnefont, J., Bali, C., Orduz, D., Bilheu, A., Herpoel, A., et al. (2013). Pyramidal neurons derived from human pluripotent stem cells integrate efficiently into mouse brain circuits in vivo. Neuron *77*, 440–456.

Gao, X., Joselin, A.P., Wang, L., Kar, A., Ray, P., Bateman, A., Goate, A.M., and Wu, J.Y. (2010). Progranulin promotes neurite outgrowth and neuronal differentiation by regulating GSK-3β. Protein Cell. *1*, 552–562.

Gass, J., Lee, W.C., Cook, C., Finch, N., Stetler, C., Jansen-West, K., Lewis, J., Link, C.D., Rademakers, R., Nykjær, A., and Petrucelli, L.

(2012). Progranulin regulates neuronal outgrowth independent of sortilin. Mol. Neurodegener. *7*, 33.

Goldman, J.S., Farmer, J.M., Wood, E.M., Johnson, J.K., Boxer, A., Neuhaus, J., Lomen-Hoerth, C., Wilhelmsen, K.C., Lee, V.M., Grossman, M., and Miller, B.L. (2005). Comparison of family histories in FTLD subtypes and related tauopathies. Neurology *65*, 1817–1819.

Hu, B.Y., and Zhang, S.C. (2009). Differentiation of spinal motor neurons from pluripotent human stem cells. Nat. Protoc. *4*, 1295–1304.

Hutton, M., Lendon, C.L., Rizzu, P., Baker, M., Froelich, S., Houlden, H., Pickering-Brown, S., Chakraverty, S., Isaacs, A., Grover, A., et al. (1998). Association of missense and 5′-splice-site mutations in tau with the inherited dementia FTDP-17. Nature *393*, 702–705.

Kayasuga, Y., Chiba, S., Suzuki, M., Kikusui, T., Matsuwaki, T., Yamanouchi, K., Kotaki, H., Horai, R., Iwakura, Y., and Nishihara, M. (2007). Alteration of behavioural phenotype in mice by targeted disruption of the progranulin gene. Behav. Brain Res. *185*, 110–118.

Kim, C. (2014). Disease modeling and cell based therapy with iPSC: future therapeutic option with fast and safe application. Blood Res. *49*, 7–14.

Korade, Z., and Mirnics, K. (2011). Wnt signaling as a potential therapeutic target for frontotemporal dementia. Neuron *71*, 955–957.

Li, H.L., Wang, H.H., Liu, S.J., Deng, Y.Q., Zhang, Y.J., Tian, Q., Wang, X.C., Chen, X.Q., Yang, Y., Zhang, J.Y., et al. (2007). Phosphorylation of tau antagonizes apoptosis by stabilizing beta-catenin, a mechanism involved in Alzheimer's neurodegeneration. Proc. Natl. Acad. Sci. USA *104*, 3591–3596.

Ming, G.L., and Song, H. (2011). Adult neurogenesis in the mammalian brain: significant answers and significant questions. Neuron *70*, 687–702.

Miranda, C.J., Braun, L., Jiang, Y., Hester, M.E., Zhang, L., Riolo, M., Wang, H., Rao, M., Altura, R.A., and Kaspar, B.K. (2012). Aging brain microenvironment decreases hippocampal neurogenesis through Wnt-mediated survivin signaling. Aging Cell *11*, 542–552.

Neary, D., Snowden, J., and Mann, D. (2005). Frontotemporal dementia. Lancet Neurol. *4*, 771–780.

Ong, C.H., He, Z., Kriazhev, L., Shan, X., Palfree, R.G., and Bateman, A. (2006). Regulation of progranulin expression in myeloid cells. Am. J. Physiol. Regul. Integr. Comp. Physiol. *291*, R1602–R1612.

Qiang, L., Fujita, R., and Abeliovich, A. (2013). Remodeling neurodegeneration: somatic cell reprogramming-based models of adult neurological disorders. Neuron *78*, 957–969.

Renton, A.E., Majounie, E., Waite, A., Simón-Sánchez, J., Rollinson, S., Gibbs, J.R., Schymick, J.C., Laaksovirta, H., van Swieten, J.C., Myllykangas, L., et al.; ITALSGEN Consortium (2011). A hexanucleotide repeat expansion in C9ORF72 is the cause of chromosome 9p21-linked ALS-FTD. Neuron *72*, 257–268.

Rosen, E.Y., Wexler, E.M., Versano, R., Coppola, G., Gao, F., Winden, K.D., Oldham, M.C., Martens, L.H., Zhou, P., Farese, R.V., Jr., and Geschwind, D.H. (2011). Functional genomic analyses identify pathways dysregulated by progranulin deficiency, implicating Wnt signaling. Neuron *71*, 1030–1042.

Takahashi, K., Okita, K., Nakagawa, M., and Yamanaka, S. (2007a). Induction of pluripotent stem cells from fibroblast cultures. Nat. Protoc. *2*, 3081–3089.

Takahashi, K., Tanabe, K., Ohnuki, M., Narita, M., Ichisaka, T., Tomoda, K., and Yamanaka, S. (2007b). Induction of pluripotent stem cells from adult human fibroblasts by defined factors. Cell *131*, 861–872.

Van Damme, P., Van Hoecke, A., Lambrechts, D., Vanacker, P., Bogaert, E., van Swieten, J., Carmeliet, P., Van Den Bosch, L., and Robberecht, W. (2008). Progranulin functions as a neurotrophic factor to regulate neurite outgrowth and enhance neuronal survival. J. Cell Biol. *181*, 37–41.

van Swieten, J.C., and Heutink, P. (2008). Mutations in progranulin (GRN) within the spectrum of clinical and pathological phenotypes of frontotemporal dementia. Lancet Neurol. *7*, 965–974.

Wexler, E.M., Paucer, A., Kornblum, H.I., Palmer, T.D., and Geschwind, D.H. (2009). Endogenous Wnt signaling maintains neural progenitor cell potency. Stem Cells *27*, 1130–1141.

Stem Cell Reports, Volume *4*

Supplemental Information

Restoration of Progranulin Expression Rescues Cortical Neuron Generation in an Induced Pluripotent Stem Cell Model of Frontotemporal Dementia

Susanna Raitano, Laura Ordovàs, Louis De Muynck, Wenting Guo, Ira Espuny-Camacho, Martine Geraerts, Satish Khurana, Kim Vanuytsel, Balazs I. Tóth, Thomas Voets, Rik Vandenberghe, Toni Cathomen, Ludo Van Den Bosch, Pierre Vanderhaeghen, Philip Van Damme, and Catherine M. Verfaillie

SUPPLEMENTAL FIGURES AND LEGENDS

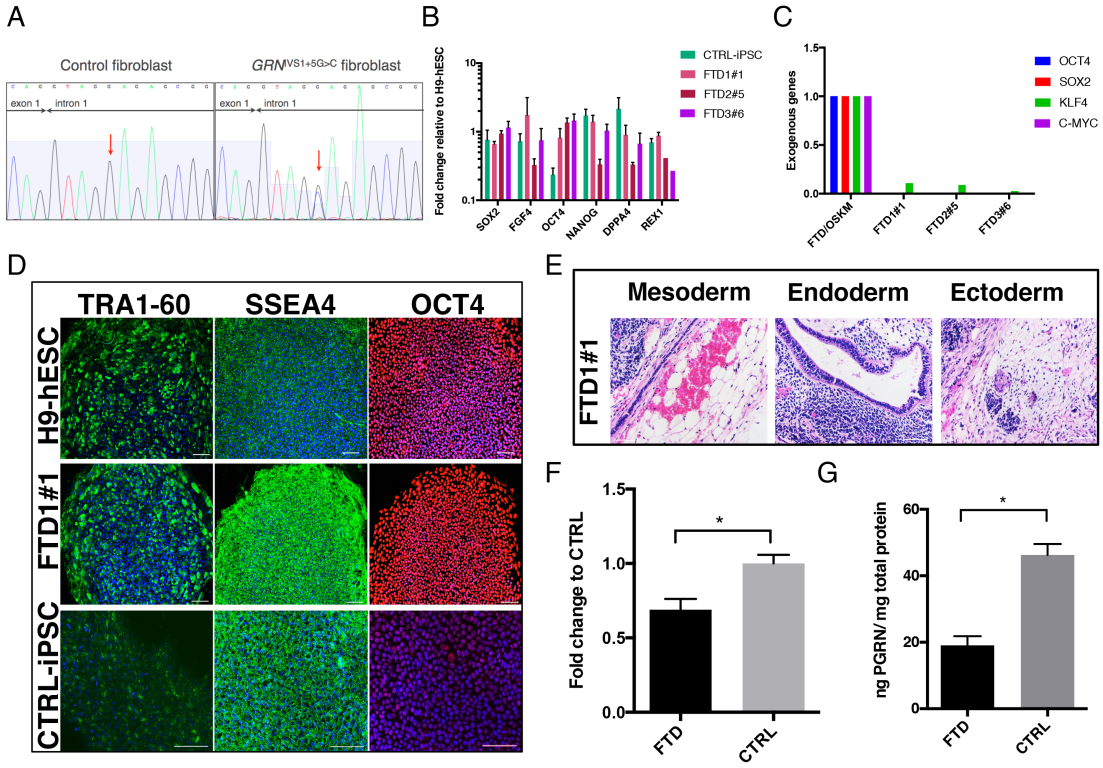

Figure S1, related to Figure1. iPSC generation from FTD patients and unaffected control

(A) DNA sequencing of the *GRN*$^{IVS1+5G>C}$ mutation in FTD-fibroblasts before reprogramming.

(B) Endogenous *SOX2, FGF4, OCT4, NANOG, DPPA4* and *REX1* transcripts levels in FTD1#1, FTD2#5, and FTD3#6 and CTRL-iPSCs cells compared to H9-hESCs (N=3 different passages. N=3 technical replicates of FTD3#6 and FTD2#5 for REX1. Error bars indicate mean ± SEM. t test analysis shows no significant differences)

(C) *OCT4, SOX2, KLF4* and *C-MYC* transgene expression in all the lines compared to the d5-transduced fibroblasts.

(D) Immunostaining for the pluripotency markers *TRA-1-60, SSEA4* and *OCT4* in H9-hESCs, FTD-iPSCs and CTRL-iPSCs. FTD1#1 is shown. (N=3 Scale bar = 100µm).

(E) Teratomas with presence of derivatives of all three germ-layers generated from iPSC lines. FTD1#1 is shown as representative of all the FTD-iPSCs.

Scale bar=500µm.

(F) Expression levels of *GRN* transcripts in FTD-iPSCs compared to CTRL lines. The average of the CTRL lines and the average of FTD-iPSC lines are shown. (N=3 different passages. Error bars indicate mean ± SEM. t test=*p = < 0.05).

(G) ELISA assay for PGRN protein in FTD-iPSCs compared to CTRL cells. The total protein was extracted from cells at three different passages; the average of the CTRL lines and the average of FTD-iPSC lines are shown. (N=3 different passages. Error bars indicate mean ± SEM. t test: *p = < 0.05).

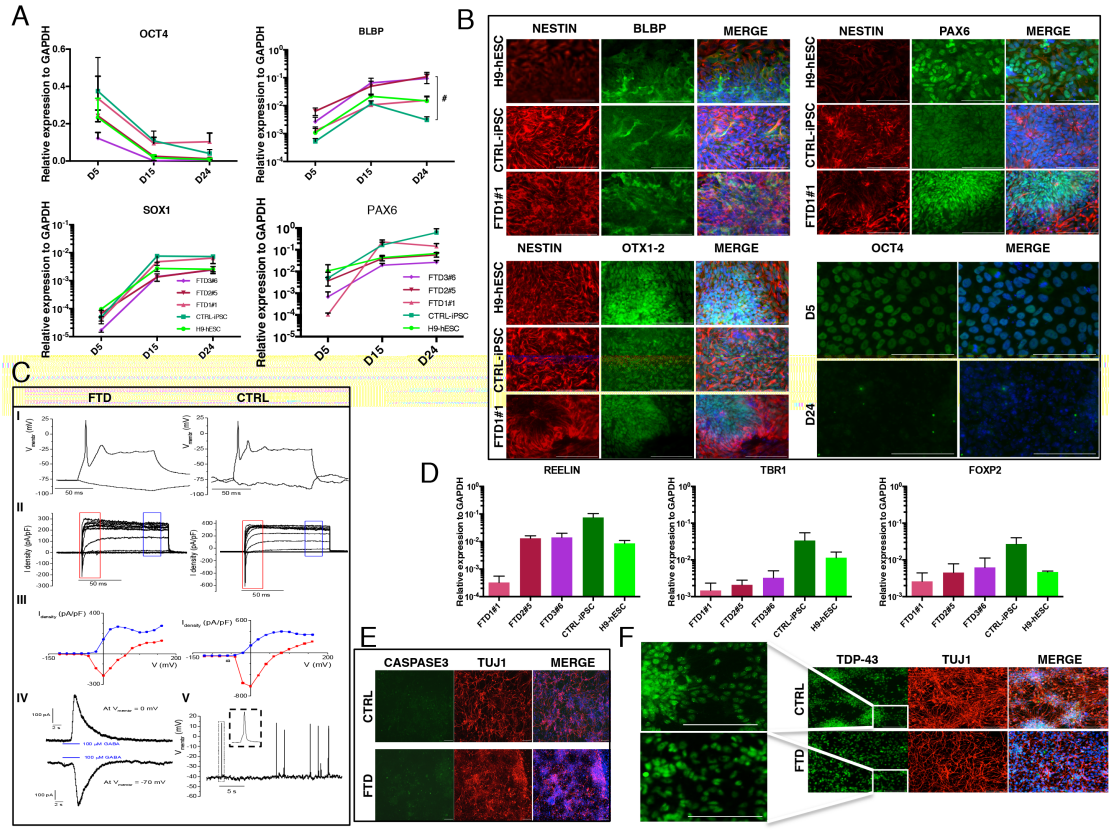

Figure S2, related to Figure1. Differentiation of hESCs and iPSCs toward neural committed cells

(A) Transcript levels for the neuro-progenitor marker genes, *BLBP, SOX1,* and *PAX*, and the pluripotency gene, *OCT4,* during differentiation of all cell lines (N=3 independent experiments. Error bars indicate mean ± SEM. t test: #= p=0.06).

(B) Representative immunostaining example of one from the three experiments performed on neural-rosettes derived from H9-hESCs, CTRL-iPSCs and FTD-iPSCs

on d24 of differentiation. FTD1#1 is shown as a representative of all the FTD-iPSC lines. (N=3 Scale bar = 100 μm).

(C) **I:** Representative action potentials evoked by depolarizing current injection on FTD (N=23) and CTRL-iPSC derived neurons (N=4 and N=5 for CTRL-iPSC-neurons and H9-neurons, respectively). **II:** Representative transmembrane currents of FTD and Ctrl-iPSC derived neurons evoked by depolarizing voltage steps from -120 to +160 mV in 20 mV steps. **III:** Negative (red line) and positive (blue line) peak currents at different membrane potentials determined in the time curse indicated on panel B. FTD2#5 iPSC and CTRL-iPSC progeny are shown. (N=17, 5 and 5 in case of FTD-iPSC-neurons, CTRL-iPSC-neurons and H9-neurons, respectively). **IV:** Representative GABA induced transmembrane currents on an FTD-iPSC derived neuron recorder at -70 and 0 mV membrane potential (N=9 of 14 cells tested). **V:** Spontaneous firing detected on an FTD-iPSC derived neuron at d40.

D) Expression levels of *REELIN*, *TBR1* and *FOXP2* of FTD-iPSC compared to CTRL-iPSC and H9-hESC lines at d40 of differentiation. (N=3 independent experiments. Error bars indicate mean ± SEM. t test analysis shows no significant differences)

(E) Immunostaining for Caspase3 on d40 progeny. FTD3#6 is shown. (Scale bar=100μm)

(F) Immunostaining for TDP43 on d40 progeny. FTD3#6 is shown. (Scale bar=100μ)

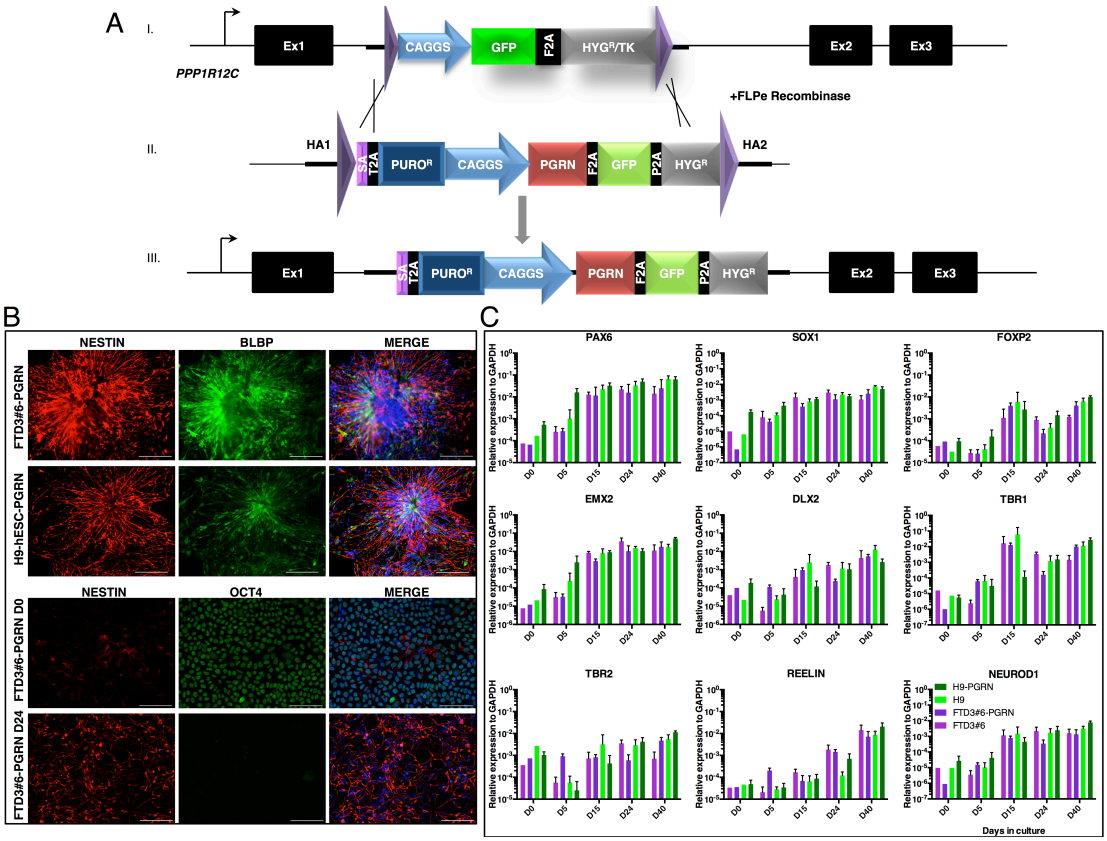

Figure S3, related to Figure2 and Figure3. Characterization of differentiation from FTD3#6, FTD3#6-PGRN, H9-hESC and H9-PGRN lines

(A) **I:** Schematic representation of RCME-H9-hESC AAVS1 locus, containing a cassette with CAGGS=chicken ß-Actin promoter, GFP=Green Fluorescent protein and $HYG^{R/}$TK=Hygromycin^{R}-thymidine kinase fusion gene flanked by FRT sequences (violet triangles). **II:** The gene-targeting vector containing the cDNA of PGRN, flanked by FRT sequences (same as in Figure 2A), which allow FLPe-recombinase mediated cassette exchange. **III:** The final recombined gene locus after integration of the cassette.

(B) Representative immunostaining example of one from the three experiments performed on neural-rosettes derived from H9-hESC-PGRN and FTD3#6-PGRN on d24 of differentiation. (N=3 Scale bar = 100µm)

(C) Transcript levels of *PAX6*, *SOX1*, *FOXP2*, *EMX2*, *DLX2*, *TBR1*, *TBR2*, *REELIN* and *NEUROD1* between d0 and d40 of differentiation for FTD3#6, FTD3#6-PGRN, H9-hESC and H9-PGRN lines. (N= 3 independent experiments. Error bars indicate mean ± SEM. t test analysis shows no significant differences.)

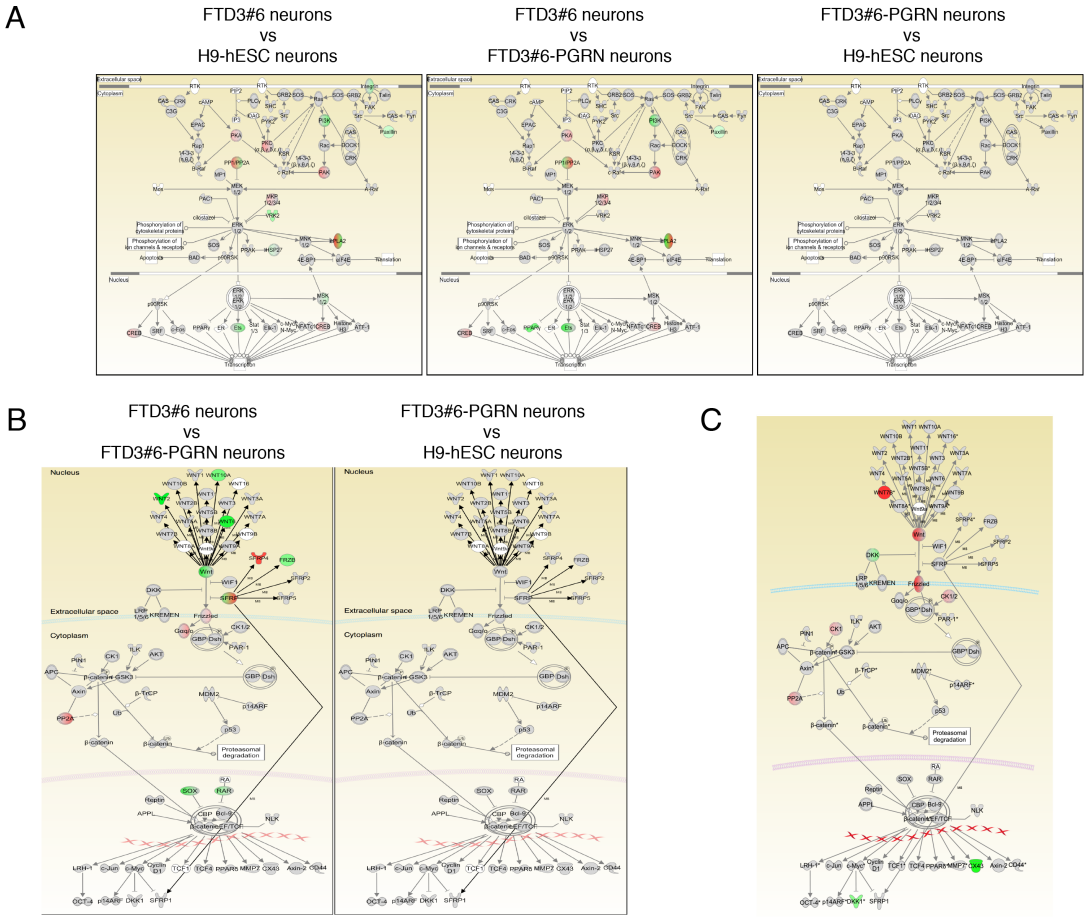

Figure S4, related to Figure4. Genome-wide transcriptome analysis of d40 neuronal progeny

(A) MAPK signaling pathway, overlaid with the differentially expressed genes (log2-ratio > 1 or < -1) of each comparison. FTD3#6 vs. H9-hESC, FTD3#6 vs. FTD3#6-PGRN and FTD3#6-PGRN vs. H9-hESC comparisons are shown. Upregulated genes are colored green and down-regulated genes are colored red.

(B) WNT signaling pathway, overlaid with the differentially expressed genes (log2-ratio > 1 or < -1) of FTD3#6 vs. FTD3#6-PGRN and FTD3#6-PGRN vs. H9-hESC comparisons. Upregulated genes are colored green and down-regulated genes are colored red.

(C) WNT signaling pathway in Almeida's paper, overlaid with the differentially expressed genes (log2-ratio > 1 or < -1). Upregulated genes are colored green and down-regulated genes are colored red.

EXTENDED EXPERIMENTAL PROCEDURES

iPSC generation

To obtain primary human dermal fibroblast cultures, skin biopsies of FTD patients carrying the *GRN*$^{IVS1+5G>C}$ mutation were obtained after informed consent; control iPSC were generated from BJ fibroblasts (Takahashi et al., 2007a). Skin biopsies were dissected into small pieces and derived fibroblast cultures were maintained in Dulbecco's Modified Eagle Medium: Nutrient Mixture F-12 (DMEM:F-12) supplemented with 10% fetal bovine serum (Greiner Bio-One), 0.016% sodium bicarbonate (Sigma-Aldrich), 1X MEM non-essential amino acids, 50 U/ml penicillin and 50µg/ml streptomycin. Human iPSC lines were generated and characterized as previously described using the four Yamanaka transcription factors (TFs) *OCT4, SOX2, KLF4* and *C-MYC* (Takahashi et al., 2007b). To exclude contamination, iPSC line identity was examined by SNP analysis. Mutation status was confirmed with a custom *GRN*$^{IVS1+5G>C}$ TaqMan SNP genotyping 2 assay and Sanger sequencing.

Teratoma formation and analysis

FTD-iPSCs, the CTRL-iPSCs and the genetically corrected FTD-iPSC were collected through enzymatic dissociation, 5-10 million cells were resuspended in 100µl PBS and injected with 100µl matrigel (Becton Dickinson, 354230) subcutaneously in the back of severe combined immunodeficient RAG2$^{-/-}$ γc$^{-/-}$ mice. These experiments were approved by the Institutional Ethics Committee.

Tumors generally developed within 4–8 weeks. Animals were sacrificed for dissection, teratomas were fixed in 4% paraformaldehyde (overnight), washed in 70%

Ethanol and subsequently embedded in paraffin. After sectioning, the presence of cells from three germlayers was assessed following hematoxylin and eosin staining.

Array Comparative Genomic Hybridization (aCGH)

Genomic DNA isolated from the three FDT-iPSC lines as well as the genetically using QiaAmp DNA mini kit (Qiagen) were subjected for CNV analysis on 180k Cytosure ISCA v2 arrays (Oxford Gene Technology, Oxford, UK).

Southern blot

Southern blot was performed to determine if random integrations occurred in the genome of FTD3#6-PGRN after FTD3#6 gene editing. Genomic DNA (5-7 µg) was digested overnight with *ECORI* and *AVRII*. The probe was designed on the homology arm 1 (HA1) so that also the FTD3#6 will be positive but the fragment would have a different size (4 Kb) than the FTD3#6-PGRN (4,7 Kb) for *AVRII* digested samples.

Differentiation of pluripotent stem cells to cortical neurons

hESC and iPSC lines were differentiated toward neural-specific progeny into 5 cm dishes (150288, NUNC) pre-coated with Matrigel (734-1440, VWR) diluted in DMEM:F-12 for 1 h at 37 °C, in a 21% O2 – 5.8% CO2 – 37°C incubator. Cells were expanded in mTeSR medium (Stem Cell Technologies, 05850) for two days in presence of ROCK inhibitor (Y-27632; 10 µM Millipore, 688001). To induce neural differentiation, medium was switched to a Defined Default Medium (DDM) (Gaspard et al., 2008) with B27 without Vitamin A (Gibco, 12587-010), supplemented with recombinant human Noggin (6057-NG, R&D Systems) for 16 days. All culture media and supplements were from Invitrogen unless otherwise stated.

The neural progenitor cells on d24 were manually dissociated and transferred on laminin/poly-D-Lysine coated glass coverslips and allowed to differentiate without medium change until d40.

In some cultures, 2μM IWP-2 (Stemgent 04-0034), which inactivates PORCN, a membrane-bound O-acyltransferase, and selectively inhibits palmitoylation of WNT, blocking WNT-dependent phosphorylation of LRP6 receptor and DVL2, and β-catenin accumulation (Kalani et al., 2008), was added during the differentiation. IWP inhibitor is reconstituted in DMSO and therefore the corresponding controls for DMSO treatment alone were taken along.

Quantitative Reverse Transcription PCR

Total RNA was extracted from human dermal fibroblasts, iPSCs and differentiated iPSCs using the RNeasy Mini kit (Qiagen). Total RNA was reverse transcribed to cDNA using SuperScript® III reverse transcriptase (Invitrogen). Quantitative PCR (qPCR) was done with SYBR Green primers and performed with Platinum SYBR green qPCR Supermix-UDG (Invitrogen) with an Eppendorf Realplex (Eppendorf). All samples were run in triplicate and relative quantification was done using the ΔΔCt method (Pfaffl, 2001) with normalization to GAPDH. Statistical analysis were performed using the Student's *t*-test, error bars show SEM. A list of primers can be found in the Table S3.

Immunocytochemistry

Immunostaining was performed by fixing the cells with 4% paraformaldehyde for 30 min or in 10% neutral buffered formalin (NBF) for 15 minutes at room temperature. Permeabilization and blocking was done for 30 min using PBS containing 3% BSA (Sigma-Aldrich, L9530), 0.3% Triton X-100 (Acros Organics) and 5% donkey serum

(Jackson). Cells were then incubated overnight at 4°C with primary antibodies (Abs) diluted in PBS with 3% BSA, 1% donkey serum, 0.1% Triton X-100. After three washes in PBS, cells were incubated with a mixture of secondary Abs and Hoechst (Sigma-Aldrich, 33258) for 90 min at room temperature. Primary Abs and dilutions are listed in the Table S4.

Western Blot

Protein was extracted from d40 cultures. 20μg of total protein was loaded and running was performed for 1h at 120 V. PVDF membrane was used for transfer, which was carried out for 1h30' at 100 V. Blocking TBS-T 5% milk was done for 1h at 4°C. Primary Ab was kept over night at 4°C and secondary Ab for 1h30' at RT.

The WB for total β-catenin WB was performed following stripping the antibody against active β-catenin.

Patch-clamp recording

Whole-cell current-clamp and voltage-clamp measurements were carried out by using an EPC-10 amplifier and Patchmaster software (HEKA Elektronik). Pipette electrodes were fabricated and fire polished with a final tip resistances 2–5 MΩ. Recordings were performed at room temperature in a bath solution containing (in mM): NaCl, 147; KCl, 2; MgCl2, 2; CaCl2, 1.2; HEPES, 10; glucose, 10 (pH 7.4) and patch pipettes were filled with a solution containing (in mM): K-gluconate, 120; KCl, 20; NaCl, 10; CaCl2, 1; EGTA, 10; HEPES, 10; Mg-ATP, 4; K-GTP, 0.1 (pH 7.2). In voltage clamp measurements, the holding potential was -70 mV, if it is not mentioned otherwise.

Gene targeting by zinc finger nuclease technology

Gene targeting was done using a dual vector, containing both the *AAVS1* homology regions and FRT sequences, suitable for gene targeting and recombinase mediated cassette exchange (RMCE)-mediated by Flipase (FLPe) (Ordovas et al., unpublished data). A copy of the *GRN* coding sequence followed by a F2A-GFP-P2A-Hygromycin cassette was cloned under the control of the *CAGGS* promoter into an AAVS1 donor plasmid flanked by heterotypic FRT sequences (p*Z:F3-P F*) (Ordovas et al., unpublished data). For gene targeting in FTD-iPSCs, the dual donor plasmid was co-transfected together with *AAVS1*-specific ZFN expressing vectors (Mussolino et al., 2014) in the FTD3#6 cell line as follows: four million iPSC were nucleofected with 10µg of gene targeting vector and 3µg of ZFN plasmids using the hESC Nucleofector Solution2, and program A23 (Lonza, Walkersville, MD) following the manufacturer's instructions. Cells were plated on inactivated DR4 mouse embryonic fibroblasts (GlobalStem, Rockville, MD) in media containing 10µM ROCK inhibitor (Sigma-Aldrich). Selection with puromycin (Sigma-Aldrich) was applied for up to one week starting from 300ng/ml increasing to 700ng/ml. Surviving colonies were individually manually selected and then expanded. Genotyping PCRs were performed according to standard procedures.

Generation of H9-hESC-PGRN was achieved by co-transfection of the dual donor plasmid and a Flippase expressing vector into an H9-hESCs, previously engineered to contain an FRT-flanked cassette into the *AAVS1* locus available in our lab. With this system, we have shown that after puromycin and 1-(2-deoxy-2-fluoro-beta-D-arabinofuranosyl)-5-iodouracil (FIAU) positive/negative selection, correct recombination in the *AAVS1* locus between the FRT sequences without random target

integrations is found in 100% of the drug-resistant colonies (Ordovas et al., unpublished data).

RNAseq analysis

Total RNA was isolated (Sigma) from two biological replicates of the FTD3#6, FTD3#6-PGRN and H9-hESC. RNA concentration, quality and integrity was determined with spectrophotometry ($A_{260/280}$, NanoDrop) and the Agilent Bioanalyzer. Library preparation was done with the TruSeq Stranded mRNA sample prep kit (Illumina) and single-end sequenced with 50bp reads on the HiSeq™2000 platform (Illumina). Raw reads were subjected to quality control. Average base quality per cycle and average read quality was calculated by the ShortRead 1.20.0 package from Bioconductor (http://www.bioconductor.org). Low quality ends (< *Q*20) were trimmed with FastX 0.0.13. Adapters were trimmed only at the end (at least 10 bp overlap and 90% match) with Cutadapt 1.2.1. Reads shorter than 35bp after adapter trimming were removed.

Preprocessed reads were mapped to the reference genome of *Homo sapiens* (GRCh37.73) with Tophat v2.0.8b, and annotated using mergeBed from the Bedtools v2.17.0 toolkit. The number of reads in the alignments that overlap with the gene features were counted using htseq-count version 2, and merged with the gene annotation. Genes with less than 1 count-per-million were removed. Statistical comparative analysis to obtain the differentially expressed genes between the different sample groups were calculated in Bioconductor. The resulting p-values are corrected for multiple testing with Benjamini-Hochberg to control the false discovery rate (FDR).

The data discussed in this publication have been deposited in NCBI's Gene Expression Omnibus (Edgar *et al*., 2002) and are accessible through GEO Series accession number GSE60902:

(http://www.ncbi.nlm.nih.gov/geo/query/acc.cgi?acc=GSE60902).

Pathway and gene ontology analysis

Gene ontology (GO) analysis was performed with the DAVID functional annotation tool (for Database for Annotation, Visualisation, and Integrated Discovery) on all significant differentially expressed genes between d40 H9-hESC neurons and d40 FTD3#6 neurons (Benjamini-Hochberg corrected $P \leq 0.05$), irrespective of the direction of the change (Huang da et al., 2009a, b). The 1979 mapped IDs were compared against the Homo Sapiens background for enrichment within the highest-level (level 5) GO categories biological processes and molecular function. Only GO categories with more than three genes were selected. The Expression Analysis Systematic Explorer (EASE) score probability, a modified Fisher's exact test that is more conservative in examining P values of gene lists for gene-enrichment analysis, was used to calculate P values with a threshold of 0.1. Ingenuity pathway analysis (IPA, Ingenuity® Systems) was performed to identify functional pathways and molecular networks. The dataset was mapped tot the IPA Knowledge Base and mapped IDs (16,170) that met the log ratio cutoff of 0.5 (both up/downregulated) were included. Significance values for the overrepresented signaling and metabolic pathways are calculated by Fisher's exact right-tailed test. The significance indicates the probability of association of molecules from the dataset with the pathway as compared to random chance alone.

ANTIBODIES USED

Primary Antibodies	Dilution	Cat Number
PAX6	1:2000	Covance, PRB-278P
NESTIN	1:1000	Covance, MMS-570P
BLBP	1:2000	Chemicon, AB9558
OTX1-2	1:2000	Chemicon, AB9566
OCT-3/4	1:2000	Santa Cruz, N-19, sc-8628
SSEA4	1µg/ml	Santa Cruz, sc-21704
TRA1-60	1µg/ml	Millipore, MAB-4360
FOXP2	1:5000	Abcam, ab16046
CTIP2	1:500	Abcam, ab18465
TBR1	1:1000	Eurogentec
Active Caspase-3	1:50	Millipore AB3623
TDP-43	1:1000	Proteintech 12892-1-AP
ß-Actin	1:2000	Biokè 49705
Active ß-Catenin	1:2000	Upstate 0566592
ßIII-Tubulin	1:2000	Covance MMS-435P
Isotypes	Cat Number	
mouse IgG1	BD Biosciences, 550878	
goat IgG	Jackson, 005-000-002	
rabbit IgG	BD Biosciences, 550875	
Secondary Antibodies	Dilution	Cat Number
D∂Rb Alexa Fluor-488	1:500	Invitrogen,A21206
D∂Gt Alexa Fluor-488	1:500	Invitrogen,A11055
D∂Ms Alexa Fluor-488	1:500	Invitrogen,A21202
D∂Ms Alexa Fluor-555	1:500	Invitrogen,A31570
D∂Rb Alexa Fluor-555	1:500	Invitrogen,A31572
D∂Gt Alexa Fluor-555	1:500	Invitrogen,A21432
Hoechst	1:1000	Sigma, 33258

PRIMERS USED

Gene	Forward primer	Reverse primer
BLBP	GGACTCTCAGCACATTCAAGAA	CCACATCACCAAAAGTAAGGGT
CTIP2	G A G T A C T G C G G C A A G G T G T T	T A G T T G C A C A G C T C G C A C T T
DLX2	ACGCTCCCTATGGAACCAGTT	TCCGAATTTCAGGCTCAAGGT
EMX2	GCTTCTAAGGCTGGAACACG	CCAGCTTCTGCCTTTTGAAC
FOXG1	GCCACAATCTGTCCCTCAACA	CGGGTCCAGCATCCAGTAG
PAX6	GTGTCTACCAACCAATTCCACAAC	CCCAACATGGAGCCAGATG
REELIN	G T A G C A A G C C C T T C A G C A A C	C C C T G A G G C C A G T A C A A C A T
SOX1	GCAAGATGGCCCAGGAGAA	CCTCGGACATGACCTTCCA
TBR1	ATGGGCAGATGGTGGTTTTA	GACGGCGATGAACTGAGTCT
GRN	GTGCCCAGATGGTCAGTTCT	CCCTGAGACGGTAAAGATGC
GAPDH	GAAGGTGAAGGTCGGAGTC	GAAGATGGTGATGGGATTTC
JA5'	CACTTTGAGCTCTACTGGCTTC	CATGTTAGAAGACTTCCTCTGC
JA3'	TTCACTGCATTCTAGTTGTGG	GGAACGGGGCTCAGTCTG
OCT4	GACAGGGGGAGGGGAGGAGCTAGG	CTTCCCTCCAACCAGTTGCCCCAAAC
DPPA4	GGAGCCGCCTGCCCTGGAAAATTC	TTTTCCTGATATTCTATTCCCAT
FGF4	CTACAACGCCTACGAGTCCTACA	GTTGCACCAGAAAAGTCAGAGTTG
NANOG	CAGCCCCGATTCTTCCACCAGTCCC	CGGAAGATTCCCAGTCGGGTTCACC
REX1	CAGATCCTAAACAGCTCGCAGAAT	GCGTACGCAAATTAAAGTCCAGA
KLF4 ex	ACGATCGTGGCCCCGGAAAAGGACC	TTATCGTCGACCACTGTGCTGCTG
SOX2 ex	GGCACCCCTGGCATGGCTCTTGGCTC	TTATCGTCGACCACTGTGCTGCTG
C-MYC ex	CAACAACCGAAAATGCACCAGCCCCAG	TTATCGTCGACCACTGTGCTGCTG
OCT4 ex	CCCCAGGGCCCCATTTTGGTACC	TTATCGTCGACCACTGTGCTGCTG

Authors contribution

C.M.V, P.V.D and planned the project. S.R, L.O., C.M.V., P.V.D., M.G., L.D.M. partecipated in the study design, planning and interpretation of the experiments. L.D.M performed the ELISA experiments, sequencing of GRN gene in iPSC and analyzed RNAseq data. K.V generated and characterized the CTRL-iPSC line. T.C. provided the AAVS1 ZFN. S.K. and L.D.M. provided scientific discussions and helped with data interpretation. P.V and E.C.I. provided a training course for cortical neuron generation and helped with the interpretation of data. B.I.T. and T. V. performed patch clamp analysis, and contributed in writing the manuscript. R.V provided patient's samples. S.R and C.M.V. wrote the manuscript.

Acknowledgments

We would like to thank the families of the patients who accepted to participate in this study. We also want to thank Mr. Javed Manesia and Dr. Maria Elena Pistoni for the critical help in review of the data; Prof Tanya Roskams for the analysis of the teratomas and Dr Anja Hasche for her expertise in WNT signaling. T.C. is a consultant for CRISPR Therapeutics. The work was supported by a Grant from FWO (G.0832) to CMV and PV, and FWO (G.0667.07) to CMV; grants from Katholieke Universiteit Leuven (EIW-B4855-EF/05/11, ETH-C1900-PF and EME-C2161-GOA/11/012) to CMV and a BELSPO-IUAP-DEVREPAIR grant to CMV.